Progress Report 2015 and Beam Request for 2016

Muon Capture on the Deuteron

The MuSun Experiment

PSI Experiment R-08-01, spokespersons P. Kammel, C. Petitjean, A.A. Vasilyev

MuSun Collaboration [1]

Petersburg Nuclear Physics Institute – University of Washington (Seattle) – Paul Scherrer Institut – University of Kentucky – Boston University – Regis University – University of South Carolina

http://muon.npl.washington.edu/exp/MuSun

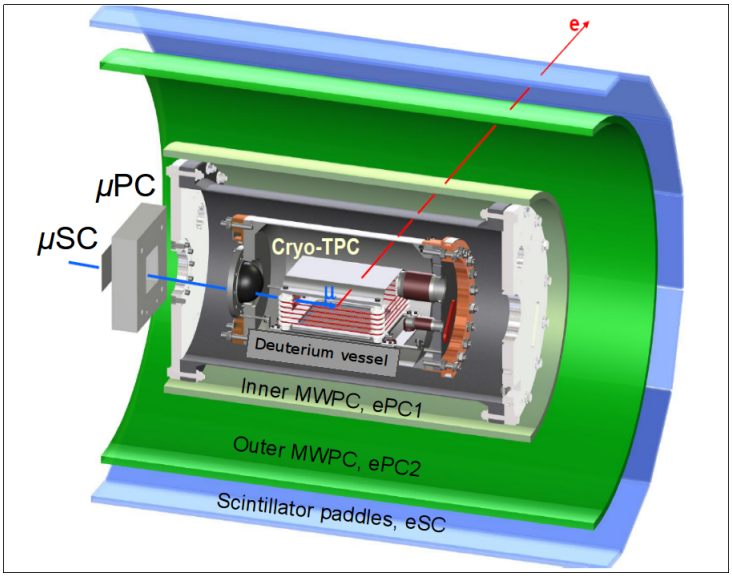

Figure 1: MuSun detector model. Muons pass through entrance detectors to stop in a deuterium target TPC. The decay electron is detected in two cylindrical wire chambers (green) and a 16-fold segmented scintillator array.

Contents

1 Overview

1.1 Introduction

The goal of the MuSun experiment is the determination of the rate of the weak semi-leptonic process

$$\mu + d \to n + n + \nu. \tag{1}$$

to 1.5% precision.

This process can be precisely calculated in the standard model, apart from a poorly known low-energy constant (LEC) involved in modern – QCD-based – effective field theory (EFT) calculations of weak nuclear reactions. MuSun plans to measure this LEC with 5 times better precision than presently available from the two-nucleon system. This LEC is an important ingredient in developing an EFT based theory of nuclear forces and is needed for calculating more complicated weak nuclear processes of topical interest, like double beta-decay rates. Regarding the family of two-nucleon weak-interaction processes, the determination of this LEC in muon capture will provide the required input for model-independent calculations of astrophysical processes of fundamental importance, like pp fusion or νd scattering, whose rates have never been measured directly.

MuSun measures Λ_d, the capture rate from the doublet hyperfine state of the muonic deuterium atom in its 1S ground state, by determining the negative muon decay rate λ_- in a time projection chamber (TPC) filled with deuterium gas. The capture rate is derived from the difference

$$\Lambda_d \approx \lambda_- - \lambda_+ \,, \tag{2}$$

where λ_+ is the positive muon decay rate.

In a simplified overview (see Fig. 1), the detector consists of muon detectors (muSC, muSCA, TPC), electron detectors (ePC1/2, eSC) and neutron detectors (not shown). For a more detailed discussion of the novel experimental strategy, we refer to our earlier Reports. The physics aspects of this field are covered in review [2].

Experimental challenges were numerous, as this program attempts to improve the measurement Λ_d by about an order of magnitude beyond earlier experiments. A key aspect was the development of the cryogenic high-density TPC operating with ultra-pure deuterium, which needed an extensive development phase, followed by significant upgrades to attain reliable operation over long running periods and excellent energy resolution.

A main step towards the experiments goal was achieved in the 2014 run, where a newly built TPC operated flawlessly over three months of data taking. The 2015 run followed suit. The TPC remained unchanged in clean conditions between the runs and worked perfectly. The purification system (CHUPS) maintained high purity at the 1 ppb level throughout the run. An improved gas chromatography (GC) produced consistent results. A method for the controlled introduction of impurities was tested after the run, and promises to calibrate the GC to better than 1 ppb. The neutron detectors were replaced with larger, high efficiency detectors, optimized for monitoring the stability of and background to the observed capture events. The πE1 beam was stable and provided a high event rate throughout the beam time, ultimately leading to 7×10^9 candidate events.

MuSun needs to measure Λ_d with an uncertainty $\delta\Lambda_d = 6$ Hz. The capture rate is derived according to equation (2), with the positive muon lifetime well-known from MuLan [3]. Thus the uncertainty in $\delta\Lambda_d$ is dominated by the MuSun measurement of λ_- in deuterium. If we assume equal statistical and systematic contributions to the final result, the statistics requirement for the number of fully reconstructed $\mu - e$ decays amounts to $\approx 1.2 \times 10^{10}$ events.

Combining the statistics of 2014 and 2015 we obtain a estimated number of 1.3×10^{10} fully reconstructed events. The statistics quoted comes from preliminary analyses. We still have to establish the final analysis cuts which might significantly reduce the statistics[1]. Nevertheless, we are optimistic that

[1] As discussed in the systematics section, the main issue is fusion interference corrections which might force a delayed fit start time.

the collected statistics comes close enough to the design goal of our experiment and the main data taking phase of MuSun is successfully concluded. The priority in the coming year will be on data analysis to fully evaluate the data consistency and the systematic uncertainties as well as the statistics after all cuts. This will determine whether systematics and statistics balance in the final result.

Thus our beam request for 2016 is very limited. We ask for a period of 4 weeks in late fall, which is dedicated to study systematic effects. We did not invest time in those studies in 2014 and 2015 and rather focused on consistent production data in uninterrupted runs.

2 Physics Run R2015

2.1 Run Overview

During the 2015 production run, over eight full weeks of μ^- data and one week of μ^+ data were accumulated. Production began on July 15th, with fine-adjustments of the beam tuning, data acquisition, and online analysis. The acquisition of production data occurred with only minor interruptions: a two day period to re-wire an electronics crate and reduce noise, and a period of time during which the electron proportional chamber gas needed to be refilled. In September, one week of μ^+ data was taken, and the last two days of beam time were used for systematics studies. Specifically, the TPC was replaced with thick scintillators to investigate electron contamination in the beam, and then replaced with various foils of commonly-used materials to investigate their muon capture signals.

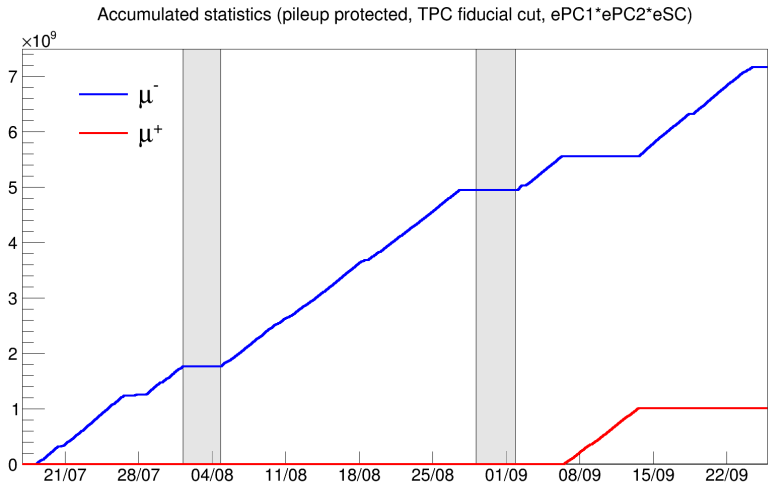

Figure 2: Number of fully reconstructed decay events acquired over the run period, after all selection cuts were applied, for R2015. The gray bands indicate the scheduled shutdown periods. The available beam was utilized with high efficiency, averaging a collection rate of $\sim 10^9$ good events per week.

In summary, the 2015 run produced more than 50 TB of data, amounting to 7×10^9 μ^- and 1×10^9 μ^+ candidate events after applying pileup protection, a fiducial volume cut, and electron tracking cuts. The accumulation of the statistics over the course of the run is shown in in Fig. 2.

Throughout production, we instituted measures to assess the integrity of the data stream. For example, we recorded timing errors in the digitizers to identify the affected runs. We also introduced a pulser to generate artificial signals in the TPC preamps with a known time signature in order to verify the time base integrity until the end of each data block. In addition, we performed separate experiments in which data were acquired from the liquid scintillator neutron detectors using a higher frequency waveform digitizer, which demonstrated improved figure-of-merit for $n - \gamma$ discrimination. These measurements motivate upgrading the DAQ and performing further systematic studies using the neutron detectors.

2.2 System Performance

2.2.1 Improved Muon Telescope

The muon entrance detectors were improved by replacing the beam defining μSCA and collimator. The μSCA, inherited from the MuCap experiment, consists of a thin scintillator with a hole in the center, and is designed to detect and veto off-axis muons. The old version used a photomultiplier tube mounted to one side to measure the muon signals, which resulted in large differences in the light collection from the near and far sides of the scintillator. The new design collects the scintillator light into two rows of silicon photomultipliers, the output of which are summed into one signal from each side, as seen in Fig. 3(a). The SiPMs are read out by variable gain amplifier and monitored by temperature sensor chips, with all electronics surface mounted on the detector support frame. The electronics is interfaced via HDMI cables to a control box, which automatically logs the temperature readings in the MuSun environmental database, and also allows for remote adjustments to the gain over the network. The new sensor configuration allows the μSCA to produce a very uniform signal regardless of the location of the event, allowing reliable discrimination between muons and electrons. The new μSCA performed well throughout the run.

The collimator was replaced with a new collimator mounted directly to the μSCA. Thus, the collimator and the μSCA are combined into one compact shielded package which can be mounted with precision and reduces the number of independent elements needed in the muon entrance detector stack. The final μSCA assembly including the collimator is shown in Fig. 3(b).

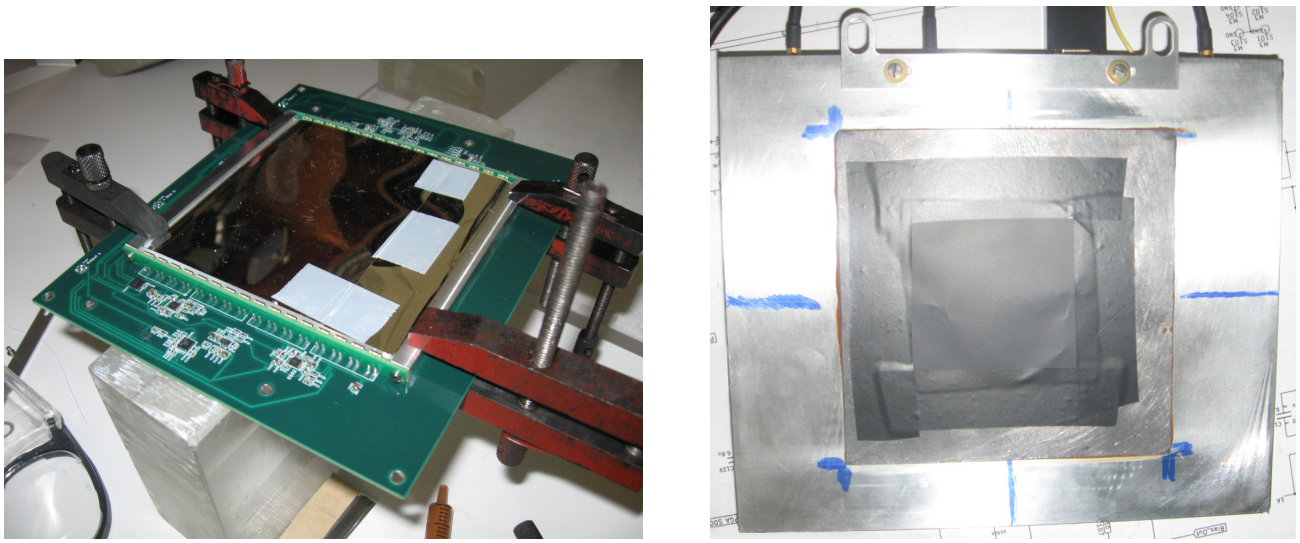

Figure 3: The new μSCA detector.

2.2.2 TPC

The TPC performed reliably throughout the run. It was operated with 80 kV across the chamber and 3.5 kV across the Frisch grid without breakdown through the run period. the top panels of figure 4 show the distribution of candidate muon stops in the TPC over the entirety of run. The TPC demonstrated excellent energy resolution due to the previously-upgraded cryogenic preamplification system. A typical energy spectrum for muon events is shown in the lower left panel of 4. The prominent peak is due to the stopped muons, with additional features due to nuclear recoil from muon catalyzed fusion appearing at higher energies. The feature at low energy is due to occasional issues with the data acquisition stream, which are straightforward to identify and remove in subsequent analysis.

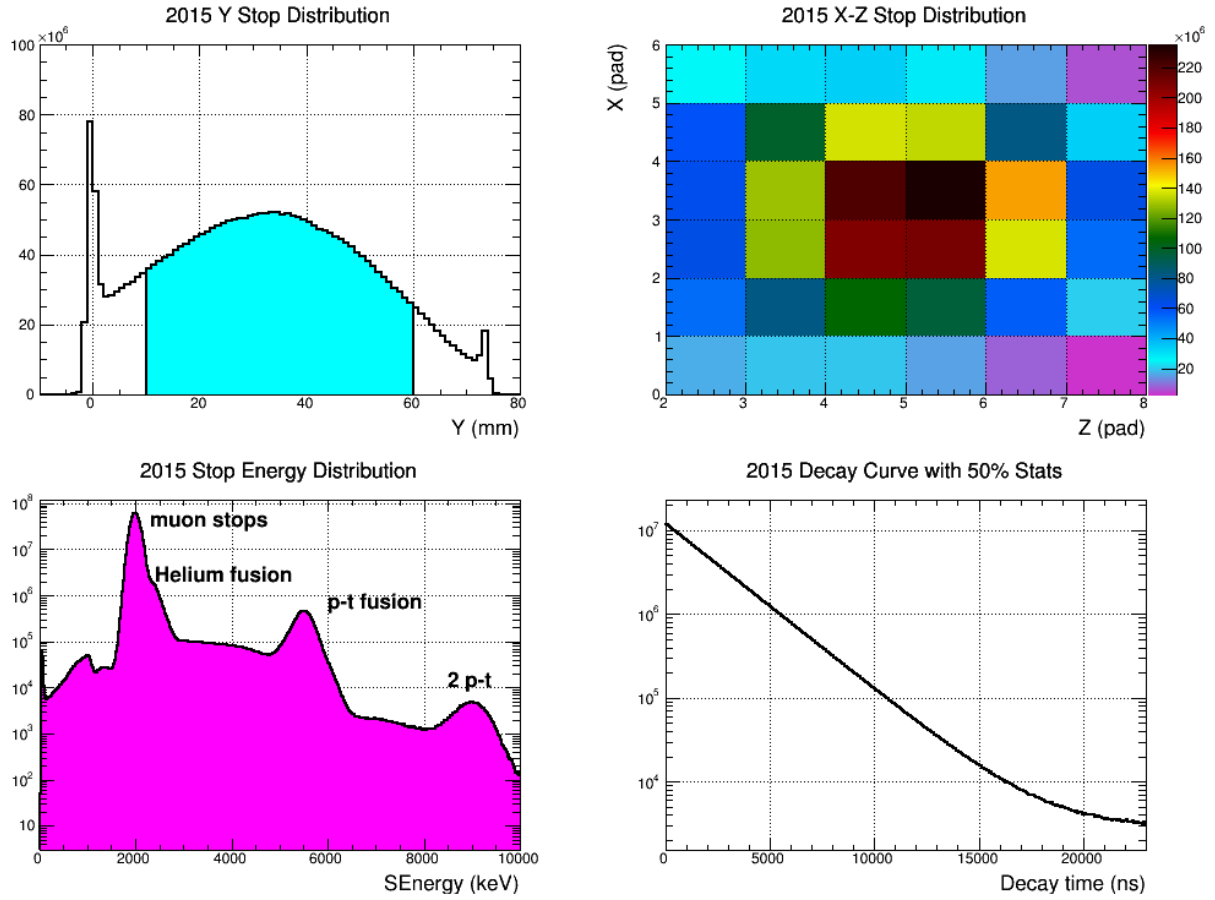

Figure 4: The stop distribution of candidate muons within the TPC in the vertical transverse direction, with shaded region representing the fiducial volume (upper left), the distribution of stops in the longitudinal and horizontal directions (upper right), the deposited energy for candidate muon stops (lower left), and a preliminary on-line analysis of the decay curve with typical cuts applied (lower right). The centrally peaked shape in the stop distribution demonstrates stable operating conditions for both the TPC and the πE1 beam throughout the 12-week campaign. All figures use approximately 50% of the total data.

2.2.3 Neutron Detectors

Muons in MuSun produce several sources of neutrons: (i) fusion neutrons following $dd\mu$ molecule formation and the subsequent $dd\mu \rightarrow {}^3\mathrm{He} + n + \mu$ fusion reaction, (ii) capture neutrons following the $\mu d \rightarrow n + n + \nu$ capture reaction and (iii) capture neutrons following muon stops in wall material.

The $d\mu d$ fusion neutrons are mono-energetic with energy 2.45 MeV. Encoded in the time dependence of the fusion neutrons are the two $dd\mu$ molecular formation rates from the $F = 1/2,\ 3/2$ hyperfine states (λ_q and λ_d) and the hyperfine transition rate (λ_{qd}) from the higher-energy $F = 3/2$ state to the lower-energy $F = 1/2$ state. Experimental verification of these kinetics parameters enables the correct extraction of the μd doublet capture rate from the decay electron time distribution.

The μd capture neutrons (ii) have a continuous energy spectrum that peaks at 1-3 MeV and extends to 53 MeV. Their intensity of 0.17% per muon is much weaker than the fusion neutron fraction of 3%. Capture neutrons are clearly separated from fusion neutrons by an energy cut above 2.45 MeV, albeit at the cost of statistics. By monitoring their intensity, impurity accumulation over the course of the run can be constrained.

Neutrons (iii) will be used to investigate background sources from muon stop in the walls and μd diffusion to the wall. As muon capture roughly scales with the 4^{th} power of the atomic number, even tiny

fractions of unidentified wall stops will increase the neutron yield. As discussed in section 3.2.2 MuSun has traded some tracking precision against reduced systematic effects from fusion interference. Thus it will be very important to quantify residual wall stops as function of tracking cuts. In order to increase the sensitivity, we will explore whether we can suppress fusion neutrons by vetoing on simultaneous He-3 signals in the TPC, which would allow us to reduce the thresholds for the neutron detectors.

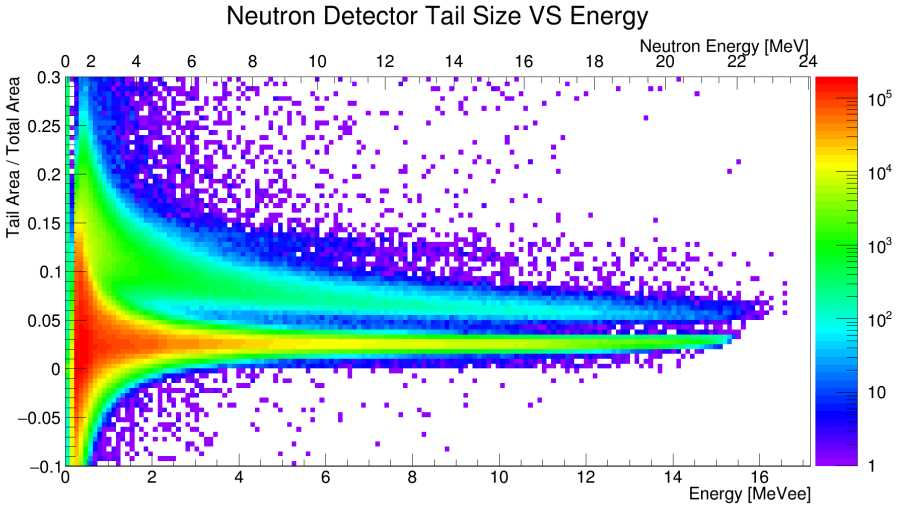

Figure 5: An example neutron PSD plot from the fast offline analysis. The upper band corresponds to neutrons, while the lower band corresponds to γ-rays

For the 2015 run, the existing detectors were replaced with large-volume neutron detectors from the DEMON collaboration, with several times higher efficiency for high energy neutrons. This allows us to observe an energy range where there are few fusions to monitor processes (ii) and (iii). All eight liquid-scintillator neutron detectors were calibrated with ^{60}Co and ^{137}Cs gamma sources. Additionally, the two time-coincident gamma rays from ^{60}Co yield a relative timing calibration. Neutron and γ-ray pulses can be distinguished on the basis of their pulse shapes. The neutron pulses have a longer tail compared to γ-ray pulses. Forming a scatter plot of the tail area compared to the total pulse area, the neutrons and γ-rays form two distinct bands as shown in Fig. 5. As the neutron spectra for wall materials are not well known, at the end of the run measurements were taken with a variety of different targets in place of the TPC to calibrate the response to background signals. An additional small scintillator was used to tag stops on the foils. Unfortunately, the neutron digitizers failed for most of these measurements, so they need to be repeated. As mentioned in sec. 2.1, we can greatly improve the $n - \gamma$ discrimination with a modest upgrade to the data acquisition, and this motivates further measurements with the neutron detectors for the purpose of quantifying systematic effects.

2.2.4 CHUPS and Chromatography

The stringent purity requirements for the MuSun experiment are achieved with the Cryogenic Hydrogen Ultra-high Purification System (CHUPS) [4]. The system actively removes contaminants with Zeolite filters, providing a continuous flow of deuterium to the TPC. The purity of the gas handling system is regularly measured using a state-of-the-art gas chromatograph (GC) capable of detecting impurities at the ppb level. It is critical to control impurities to this level: In 2013 we performed the first measurement of the muon transfer rate from deuterium to nitrogen at low temperatues and calibrated the effect of N_2 on the capture rate extraction with specifically impurity doped TPC fillings. The resulting correction to the doublet capture rate is ≈ 3 s^{-1} per ppb N_2, which implies that the purity of the system should be established to 0.5 ppb. The GC analysis was recently improved, leading to greater consistency and more

robust uncertainty estimates for chromatograph signals. CHUPS operation was stable, with impurities concentrations around 1.3 ppb throughout the run. The GC measurements over the course of the run are shown in fig. 6. The impurity levels measured throughout the run were cross-checked by regenerating the Zeolite filters and discharging most of the accumulated impurities. The measured amount of accumulated nitrogen was consistent with the GC readings.

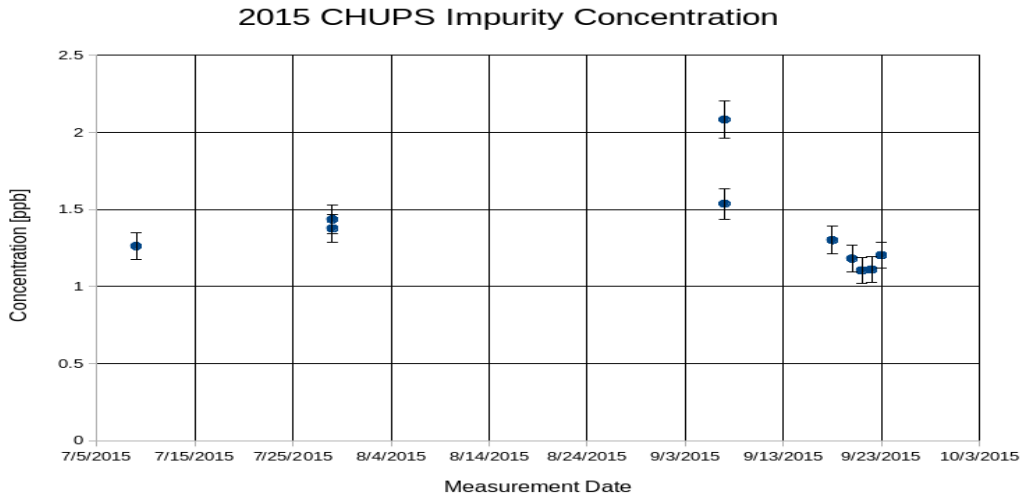

Figure 6: The measured impurity of the CHUPS system over the course of the 2015 run. The error bars reflect the uncertainty from the GC analysis software. The higher points between 9/3/2015 and 9/13/2015 are likely not due to increased impurity levels in the TPC, but rather due to the use of insufficiently-cleaned sample lines.

At the end of the run campaign, an extensive calibration program for the GC was carried out. This was performed by dynamically mixing a small additional deuterium flow with 3.22 ± 0.23 ppm of impurities into the highly-purified CHUPS system. With the aid of high-precision mass-flow controllers, this small additional flow is diluted reliably and predictably to the ppb level, and the calculated level of impurity is compared to the GC readout for calibration. These measurements were performed for various sample volumes, which demonstrated the consistency of the technique, and a preliminary analysis shows that CHUPS sensitivity will be below the level of 1 ppb as desired.

3 Data Analysis

3.1 Analysis Overview

Independent analyses are being performed by PNPI and UW. In addition, the development of the sophisticated MuSun analysis framework has lead to three recent PhD theses, which include extensive studies of systematics and a detailed analysis of muon kinetics in the TPC [5, 6, 7].

A complete analysis is under way for all MuSun production data. In 2015, the analysis software was upgraded to include more robust data quality checks (in particular the error checking of the data acquisition). In addition, the software for event selection using the entrance scintillators and proportional chamber was redesigned, along with an analysis of the muon entrance efficiency, pileup detection efficiency, and assessment of detector deadtime.

R2011 was our initial data run, and the results of this run guided critical upgrades for the R2014 and R2015 runs. Analysis of the R2011 data has shown that flexibility in the fiducial volume cuts in the TPC is necessary to reduce the systematic lifetime distortion from muon-catalyzed-fusion ("fusion interference"). This motivated the use of high-Z materials for the walls and wires of the TPC where

muons could potentially stop and capture with a dangerously different lifetime. This way, muon captures happen quickly and don't impact the decay time distribution arising from good stops. Additionally, the potential for *in-situ* detection of gas impurities using the TPC response to muon capture on nitrogen nuclei was determined by this data set, motivating the resolution upgrades for the read-out electronics and resulting in an independent measure of the gas impurity. Since the TPC underwent many upgrades following R2011, analysis of this dataset has been focussed on solving problems like fusion interference that are just as prevalent in later runs.

In December 2015, a first production pass of R2014 data was processed through the updated MuSun analysis framework, resulting in $4{\times}10^9$ muon-electron pairs which pass all quality cuts. Initial lifetime fits to the high statistics output reveal no irregularities in the fit residuals using standard analysis cuts. In addition, the decay curve is fitted while scanning various muon-electron pair cut parameters, and these studies can be used to quantify the sensitivity of the result to the final cuts. A clocked dataset from R2014 was fully analyzed to evaluate the inefficiencies of the muon entrance detectors. The analysis demonstrated a combined entrance inefficiency of 10^{-5}, leading to a lifetime shift 0.09 Hz. With the updated error checking, this first analysis revealed approximately 10% of the R2014 data contained errors in the TPC digitizer readout.

A rapid on-line analysis of approximately 50% of high quality production runs from 2015 has been performed. The bottom right panel of fig. 4 shows the muon decay curve for all of these runs, which shows no systematic distortion of the fit residuals. For 2016, The MuSun collaboration has received a grant from the Texas Advanced Computing Center for 320k CPU hours, a two-fold increase in computing time compared to 2015.

3.2 Update on Systematics

3.2.1 Purity

As mentioned in section 2.2.4, impurity levels (particularly N_2) must be controlled at or below the 1 ppb level in order to make the effect on the capture rate acceptable. This was the case for 2014 and 2015 production running. In addition to the GC measurements, the TPC is sensitive to the recoiling daughter carbon ions from μ^- capture on N_2. The analysis of carbon-recoil events, developed for previous production running, was performed online throughout the 2015 campaign as an additional monitor of the purity. The recoil signal has to be separated from the ubiquitous He-3 fusions at higher energies and Michel electrons at low energies (see figs. 10 and 11 in last year's progress report). The remaining background comes from a rare and surprising source, the $\mu + d$ capture reaction itself. The TPC acts as an efficient neutron detector and recoiling deuterons after neutron scattering contribute at a similar level as the carbon recoils in the relevant energy range. If this neutron-related and other backgrounds can be sufficiently understood, the sensitivity of this *in situ* method could approach 0.5 ppb. This would provide a direct and robust means of controlling the uncertainty on the final result for the doublet capture rate. Regardless of the systematic uncertainties related to background, it offers a stable run-by-run signal which can be used to check the impurity evolution for all production data and between different campaigns.

An important ingredient for such analyses is the detailed understanding of the TPC response. In this respect, the He-3 energy spectrum remained a persistent puzzle; it has a sharp edge at the high energy side, but a long tail at low energies, interfering with the carbon capture signal (see fig 7). This is possibly related to the significant initial electron-ion recombination in the high density TPC. For the 2014 and 2015 campaigns neutrons in the gondolas were selected which determined the direction of the ^3He in the $d\mu d \rightarrow n + {}^3He$ muon catalyzed fusion reaction. By selecting neutrons in the horizontal gondolas, ^3He that are perpendicular to the drift field direction are selected. Selecting neutrons in the vertical gondolas corresponds to angles from 0 to 50° degrees. Thus the dependence of the electron-ion recombination on the angle of the ion with respect to the drift field was quantitatively established.

An improved understanding of the impurity recoil signal comes from selecting events in coincidence with neutrons. In the 2013 campaign we had runs with very high nitrogen impurity levels which allowed

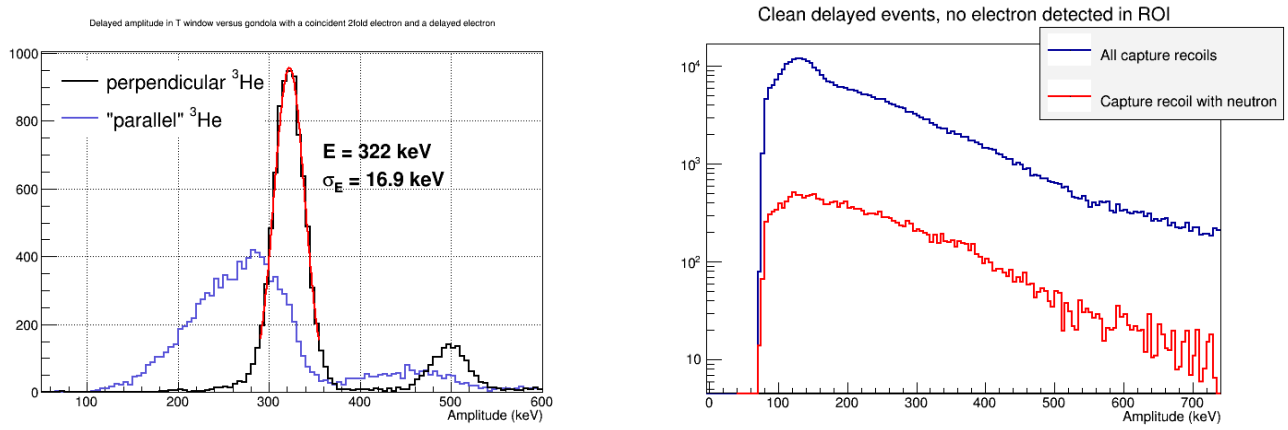

Figure 7: Left panel: ^3He recoil direction tagged by gondola neutron showing electron-ion recombination dependence on angle to drift field direction. When neutrons are selected in the horizontal gondolas the ^3He direction is nearly perpendicular to the drift field. For neutrons in the vertical gondolas the range of ^3He angles is from 0 to 50°. Right panel: Recoil spectra without and with neutron tag. Recoils in coincidence with a neutron are part of a multi-body final state and have a broad energy spectrum while recoils from a two-body final state have a sharp energy peak.

us to get a nearly pure impurity energy spectrum which has a significant peak between 100 and 200 keV. When requiring a neutron in coincidence we select for a multi-body final state and the peak is smeared out. With a dedicated set of doped measurements, the signal could be better calibrated and compared with the GC method. The neutron-related background (which is estimated to contribute to $\sim 50\%$ of the signal at low concentration) could be assessed with further systematic studies: in particular by operating the TPC when doped with known concentrations of N_2, and by using a more finely-grained TPC to reduce the sensitivity to the neutron recoil background.

3.2.2 Interferences

Muon-catalyzed fusion processes result in additional charged particle tracks in the TPC, potentially interfering with the muon track and changing the acceptance of a decay event. Because events with a fusion imply muon decay times that are later than average, this efficiency discrepancy can lead to a systematic lifetime shift. To avoid this, we have developed several muon-tracking algorithms that can identify when a muon stops in the fiducial volume of the TPC while remaining insensitive to the presence of fusion products. These algorithms use the principle that the stop position can be determined using only pulse information on pads upstream from the stop location, albeit with reduced position resolution. Using Monte Carlo simulations of fusion events, including the details of the TPC response, we can quantify the size and direction of tracking errors caused by fusion products for each of these algorithms.

The reconstruction by different algorithms relative to the truth information is compared in fig. 8. The difference between red and black is where the fusion causes a significant reconstruction error. In the left figure, the algorithm misconstructs tracks with upstream-going protons as having stopped one pad too early. In the right figure, the algorithms use energy information on the last two pads to discriminate events where the proton goes upstream vs downstream. This makes fewer mistakes overall, and in both directions.

Since all events in the fiducial volume are accepted, only tracks that are reconstructed on the wrong side of a fiducial boundary due to fusion can affect the acceptance efficiency. We call these errors "fusion migration" to indicate that the net change in the number of events accepted depends on the population of muons stopping near the fiducial boundaries. We relate the number of fusion migration events to the population near the boundary by constructing many sub-volumes of the TPC and examining the

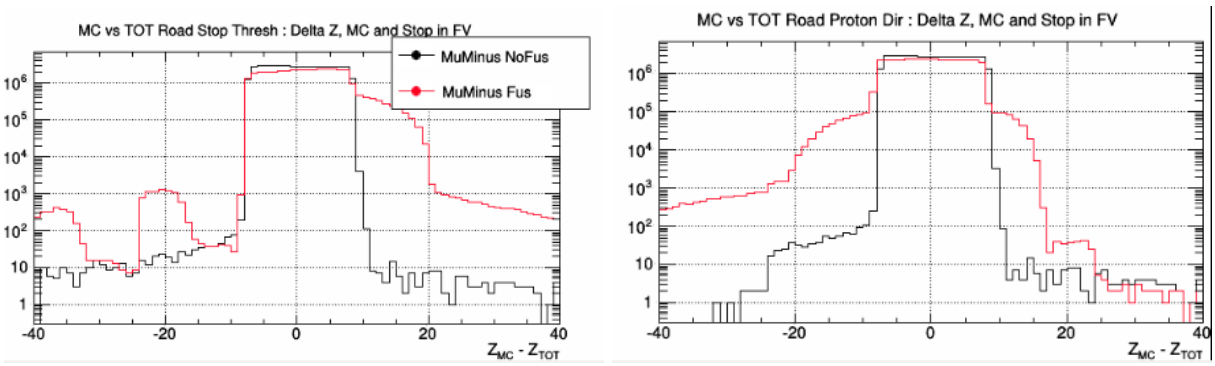

Figure 8: Comparison of algorithms for determining the z-coordinate of the muon stop using MC data. The histograms show the difference between the true muon stop point and the point reconstructed by the tracking algorithms. The black points are from control data where the energy deposition of fusion products is removed in the simulation, showing the 16 mm anode pad structure. The red points are simulation data with fusion process turned on.

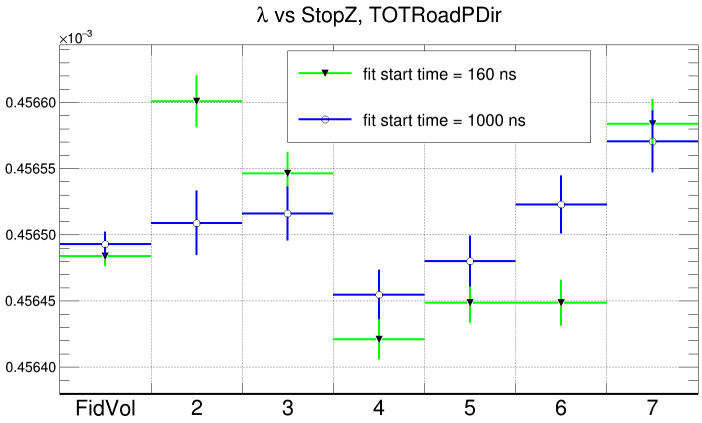

Figure 9: Fitted (blinded) disappearance rate as a function of the z-coordinate of the muon stop position (binned by TPC anode pad). The smaller volumes of this subdivision enhance the fusion migration relative to the "bulk" events. The later fit start time of 1000 ns greatly reduces the effect of fusion interference.

distortion of the decay time distribution.

Muon-catalyzed fusion occurs more often from the quartet hyperfine state, which is depopulated in 500 ns. Thus, by starting the lifetime fit at 1000 ns, we can greatly reduce the effect of fusion interference. We have applied all tracking algorithms to the full R2011 dataset and found that the algorithm designed to have the least fusion migration results in little distortion to the measured lifetime over TPC sub-volumes. Other tracking algorithms introduce larger distortion from fusion interference in the ways we expect from the simulation results. We are attempting earlier fit start times in order to maximize statistics while remaining insensitive to fusion interference.

4 Beam Time Request 2016

We request a 4 week period late fall 2016 in the πE1 area to perform final systematic studies with the MuSun set-up. This systematic run should be performed this year, where the team expertise is still available, but done late, so that the ongoing data analyses are well advanced and can prioritize the required studies.

At the moment we are considering three different topics which would benefit from special studies.

Wall stops: Effects introduced by muons stopping in wall material or $d\mu$ atoms diffusing to the walls, which have been misidentified as stopping in the fiducial volume, have not been fully assessed yet. Such corrections will be made based on the neutrons observed in the large volume neutron detectors. Their response to the unknown emission spectrum following muon capture in several target materials still has to be calibrated with dedicated target runs. PSI has expressed interest to attract large Ge detectors for different research topics. By using a 75% Ge detector in close proximity to the TPC, we could identify the composition of wall stops to below the 10^{-3} level.

Impurity calibration. The new dynamic purity calibration without beam worked very well. Measuring the TPC recoils simultaneously would allow for an absolute calibration of the system, directly based on the cold volume conditions. Such a measurement is attractive if the background from neutron scattering in the TPC can be sufficiently suppressed. Currently two methods are under study towards this goal: An X-ray coincidence requirement would essentially eliminate all background, albeit at a loss of statistics. A finer pad segmentation of the TPC would reduce the neutron scattering volume, thus improving signal to background.

Additional μ^+ statistics: In a one month run we could double our μ^+ statistics. Being free of capture and fusion complications, this data plays an important role to check physics and experimental effects, and can be compared to the 1 ppm MuLan result. Specifically, time distortions due to the interference between drifting muon tracks and decay electron signals in the TPC can be quantified; many dangerous instrumental effect for a precision lifetime measurement, like coherent baseline variations and digitizer problems, can be identified.

Pending the ongoing analysis work, we will determine the balance between the different studies before the run. As there will not be enough time for all studies in the requested month, we expect that some of the issues mentioned above can be solved within our excellent production data.

References

[1] MuSun Collaboration (http://muon.npl.washington.edu/exp/MuSun):
V.A. Andreev, E.J. Barnes, R.M. Carey, V.A. Ganzha, A. Gardestig, T. Gorringe, F.E. Gray, D.W. Hertzog, M. Hildebrandt, L. Ibanez, P. Kammel, B. Kiburg, S.A. Kizilgul, S. Knaack, P.A. Kravtsov, A.G. Krivshich, K. Kubodera, B. Lauss, M. Levchenko, X. Luo, K.R. Lynch, E.M. Maev, O.E. Maev, F. Mulhauser, M.H. Murray, F. Myhrer, K. Neely, A. Nadtochy, C. Petitjean, G.E. Petrov, J. Phillips, R. Prieels, D. Prindle, N. Raha, R. Ryan, G.N. Schapkin, N. Schroeder, G.G. Semenchuk, M.A. Soroka, V. Tishchenko, A.A. Vasilyev, A.A. Vorobyov, N. Voropaev, M.E. Vznuzdaev, F. Wauters, P. Winter.

[2] Kammel, P. and Kubodera, K. *Annu. Rev. Nucl. Part. Sci.* **60**, 32753 (2010).

[3] Tishchenko, V. et al. *Phys. Rev.* **D87**(5), 052003 (2013).

[4] Alekseev, I. e. a. *Rev. Sci. Instrum.* **86**, 125102 (2015).

[5] Ibanez, L. PhD thesis, Boston University, (2015).

[6] Luo, X. PhD thesis, Boston University, (2016).

[7] Raha, N. PhD thesis, University of Kentucky, (2015).